Collisionless electron cooling in a plasma thruster plume: experimental validation of a kinetic model

Mario Merino, Pablo Fajardo, Gabriel Giono, Jón-Tómas Gudmundsson, Nickolay Ivchenko, Stéphane Mazouffre, Dimitry Loubère, Käthe Dannenmayer

Collisionless electron cooling in a plasma thruster plume: experimental validation of a kinetic model

Mario Merino* and Pablo Fajardo
Equipo de Propulsión Espacial y Plasmas (EP2), Universidad Carlos III de Madrid, Leganés, Spain

Gabriel Giono, Jón Tómas Gudmundsson, and Nickolay Ivchenko
Department of Space and Plasma Physics, School of Electrical Engineering, KTH, Stockholm, Sweden

Stéphane Mazouffre
Institut de Combustion Aérothermique Réactivité et Environnement (ICARE), CNRS-University of Orléans, France

Dimitry Loubère
Airbus Defense and Space (Airbus-DS), Toulouse, France

Käthe Dannenmayer
European Space Research and Technology Centre (ESA/ESTEC), Noordwijk, The Netherlands

A central challenge in the modeling of the near-collisionless expansion of a plasma thruster plume into vacuum is the inadequacy of traditional fluid closure relations for the electron species, such as isothermal or adiabatic laws, because the electron response in the plume is essentially kinetic and global. This work presents the validation of the kinetic plasma plume model of Plasma Sources Sci. Technol. 27 (2018) 035013 against the experimental plume measurements of a SPT-100-ML Hall effect thruster running on xenon of Plasma Sources Sci. Technol. 27 (2018) 015006. The model predictions are compared against the axial profiles of electric potential, electron density, and electron temperature, and the radial electric potential profile, for 6 different test cases, in a region between 0.5 m and 1.5 m away from the thruster exit. The model shows good agreement with the experimental data, and the extrapolation of the model to the thruster exit plane and far downstream are consistent with the expected trends with varying discharge voltage and mass flow rate. The lumped-model value of the polytropic cooling exponent γ is similar for all test cases and varies in the range 1.26–1.31.

I. INTRODUCTION

The interaction of the plasma thruster plume with the surrounding elements of the spacecraft poses a major concern for the integration of electric propulsion systems like gridded ion engines (GIT) and Hall effect thrusters (HETs) in space missions[1–3]. The main threat are the charge-exchange ions generated in the plume near-region, which can impinge on neighboring surfaces and interact mechanically, electrically, or chemically with them. These ions originate from collisions between primary ions and low-velocity neutrals outside of the thruster, and their motion is dominated by the local electric field. For this reason, determining accurately the electric potential in the plume near-region is a key step toward the predictive simulation of charge-exchange ion effects.

The electric potential map $\phi(\boldsymbol{x})$ arises from the expansion of the primary ions and the neutralizing electrons, but depends especially on the electron thermodynamics, i.e., on the evolution of the electron temperature T_e in the plume, with hotter electrons leading to larger electric fields ($\Delta\phi \sim T_e/e$). Due to computational constraints, the majority of existing simulation codes follow a fluid description for the electrons, using a simple electron cooling law in the form $T_e \propto n_e^{\gamma-1}$ as the closure relation, where n_e is the electron density and γ is a polytropic exponent. The limit $\gamma = 1$ means an isothermal electron expansion and results in Boltzmann's relation. Unfortunately, in the near-collisionless regime of plasma thruster plumes, the fluid approach is unjustified, and a fully kinetic model must be used to obtain physically-correct solutions. The inadequacy of the fluid approach is evidenced, in particular, in the case of an isothermal electron species, which leads to an infinite potential fall as the electron density drops to zero. Moreover, even accepting the fluid approximation and a polytropic closure with $\gamma > 1$, the parameter γ must be regarded as an extra degree of freedom of the fluid model, which has to be determined for each thruster and each operating condition, bringing an additional source of uncertainty to the simulations.

In order to address these shortcomings, a kinetic electron model for plasma plumes expanding into vacuum [4] (and the open-source AKILES code[5]) was recently developed to compute self-consistently the near-collisionless electron expansion. The results of this model show the gradual electron cooling and development of anisotropy in the plume, and can be used to inform existing plume/spacecraft interaction codes like EP2PLUS[6] or SPIS[7], providing more accurate electron fluid closure relations than the currently-used isothermal and polytropic laws,

* mario.merino@uc3m.es; http://ep2.uc3m.es

or at the bare least, choosing a value for γ that is consistent with the kinetic electron response.

As with any physical model, contrasting the predictions of the kinetic model against actual experimental measurements is a necessity to validate it and gain confidence on its accuracy. To this end, a set of dedicated experiments on the plasma plume of a HET have been carried out at ESA-ESTEC, which were reported in references [8, 9]. The present paper compares the kinetic model with those experimental results, analyzing the differences found for six different thruster operating conditions. The validity of the model, and its different predictions, for these operating points is assessed by comparing the axial plasma profiles of the model and the experiments. The paper concludes with the estimation of the polytropic cooling exponent γ in the different experimental cases, as this parameter is widely employed in current simulation codes, and discusses the limitations of such single-γ approximations to model the electron response in plasma thruster plumes.

The rest of the paper is structured as follows. For the sake of self-containment, Section II summarizes the hypotheses and the main aspects of the electron kinetic model of [4]. Likewise, Section III reviews the experiments of [9]. Section IV explains the comparison procedure followed, and presents the comparison results to determine the error of the model. The discussion of the effective polytropic fluid closure law as an approximation to be used in fluid electron models is then carried out in Section V. Finally, the main conclusions of this work are gathered in Section VI.

II. KINETIC PLASMA PLUME MODEL

The model of [4] describes the steady state expansion into vacuum of a plasma jet composed of singly-charged ions and electrons. The reader is directed to that reference for a full account of the model derivation; in this section, only the major aspects of the model, such as its assumptions and parameters, are summarized.

The plasma plume is considered to be collisionless, quasineutral, unmagnetized, and slowly-diverging (i.e., paraxial). The electric potential ϕ is assumed to decrease monotonically downstream and radially, and is modeled as

$$\phi(x,r) = \phi_x(x) - \frac{C}{h(x)^4} r^2, \tag{1}$$

where C is a constant, and $\phi_x(x)$, $h(x)$ are a slowly-varying functions of x to be determined as part of the solution, which represent the potential along the plume axis ($r = 0$) and the radial widening of the plume as it expands. In essence, expression (1) prescribes the shape of the radial profile for ϕ to be parabolic. The resulting electric field $-\nabla\phi$ causes a small acceleration on the already-hypersonic ions that stream out of the thruster, and effectively confines most of the electrons, except for the highest-energy tail of their distribution. These free, escaping electrons are responsible for balancing out the ion current in the plume, making it globally current-free. A typical confined electron trajectory involves many radial reflections between two axial reflections.

Under these conditions, the mechanical energy E, the angular momentum about the plume axis p_θ, and the adiabatic invariant given by the radial action integral [10] J_r of each individual particle,

$$E = \frac{1}{2}mv^2; \qquad p_\theta = mrv_\theta; \qquad J_r = \oint mv_r \mathrm{d}r, \tag{2}$$

are conserved. The latter integral accepts a closed form, $J_r = J_r(x, r, v_r, v_\theta)$.

Ions are treated as a cold species, and their bulk density and velocity are integrated directly from their continuity and momentum equations, expressions (32) and (33) in reference [4], whereas the electron distribution function $f_e = f_e(x, r, E, p_\theta, J_r)$ is averaged over the radial electron motion into $\bar{f}_e = \bar{f}_e(x, E, p_\theta, J_r)$ and solved for using the paraxial Vlasov equation,

$$v_x \frac{\partial \bar{f}_e}{\partial x} = 0. \tag{3}$$

This equation states that $\bar{f}_e$ is constant along x for each (E, p_θ, J_r), as long as $v_x \neq 0$. The condition $v_x(x, E, p_\theta, J_r) = 0$ defines the turning manifold at which electrons are axially reflected, and is given by

$$E - U_{\mathrm{eff}}(x, p_\theta, J_r) = 0, \tag{4}$$

where U_{eff} is an effective potential for the axial motion of the electrons,

$$U_{\mathrm{eff}}(x, p_\theta, J_r) = -e\phi_x(x) + \sqrt{\frac{2eC}{m_e}} \frac{J_r/\pi + |p_\theta|}{h^2}. \tag{5}$$

Observe that the turning manifold depends on J_r and p_θ only through $p_\perp = J_r/\pi + |p_\theta|$, which allows to reduce the dimensionality of the model.

The manifold in equation (4) splits the electron phase space into four distinct regions, according to the connectivity of electron trajectories with the boundaries of the domain ($x = 0$ and $x = \infty$): (i) reflected electrons, i.e., low-energy electrons that are emitted from the plasma source and eventually reflected back to it by the potential fall along the plume; (ii) free electrons, i.e., high-energy electrons emitted from the source that can reach infinity downstream; (iii) doubly-trapped electrons, i.e., isolated electrons whose trajectories do not connect neither with $x = 0$ nor with $x = \infty$; and (iv) empty regions, which connect only with $x = \infty$ and are therefore not occupied.

At the upstream boundary ($x = 0$), conditions on the ion density n_{i0} and axial bulk velocity u_{i0} must be provided. Likewise, the forward-going ($v_x > 0$) part of the radially-averaged electron distribution function $\bar{f}_e$ is required at that position. In the present work, a semi-Maxwellian electron population is prescribed. These

boundary conditions suffice to obtain the solution of the reflected and free electrons, but additional information is required to solve for the isolated doubly-trapped population. The model assumes that either the transient set-up process of the plume [11] or the occasional collisions help populate these regions with a fraction α of the same distribution as in other electron regions.

After assuming an initial guess for the $\phi(x)$ and $h(x)$ functions, the ion and electron models are used to obtain the ion and electron density n_i and n_e along the plume axis. The quasineutrality condition, $n_i - n_e = 0$ and the current-free condition $n_i u_i - n_e u_e = 0$ are then used to compute the error of the solution and set up an iterative scheme that allows to find the self-consistent solution for $\phi(x)$ and $h(x)$.

The resulting model has three remaining degrees of freedom, which can be parametrized as the filling parameter α that characterizes the doubly-trapped electron regions; the initial ion Mach number, M_{i0}; and the square root of the ion-to-electron mass ratio μ:

$$\alpha; \qquad M_{i0} = \frac{u_{i0}}{\sqrt{T_{e0}/m_i}} \qquad \mu = \sqrt{\frac{m_i}{m_e}} \tag{6}$$

In this work, $\alpha = 1$ is chosen (fully occupied doubly-trapped regions), and $\mu = 2.39 \cdot 10^5$ (xenon). Observe that T_{e0} and n_{e0} depend on the backward-going part of the distribution function $\bar{f}_e$ at $x = 0$, which is not known a priori and must be computed as part of the solution. Finally, note also that the initial values of $\phi_x(x)$ and $h(x)$, i.e. ϕ_0 and h_0, as well as the constant C introduced in (1), can be fixed after solving the model, as long as the solution is rescaled appropriately.

III. PLASMA PLUME MEASUREMENTS

This section overviews the main aspects of the experimental campaign carried out in April-May 2017 at the ESA/ESTEC Electric Propulsion Laboratory. The measurements have been obtained in the plume of a 1.5 kW-class SPT-100-ML Hall thruster [9]. A more detailed account of the experiments can be found in that reference. The plasma properties of the plume were mapped for six different operating points of the thruster by changing the discharge voltage and the mass flow rate of Xenon to: A) 150 V, 2 mg/s; B) 225 V, 2 mg/s; C) 300 V, 2 mg/s; D) 400 V, 2 mg/s; E) 150 V, 4 mg/s; and F) 300 V, 4 mg/s. The six cases are shown in I. Two different probe diagnostics were used in the campaign: cylindrical Langmuir probes and Faraday cups.

Cylindrical Langmuir probes (5 mm long Tungsten wire with a 0.2 mm diameter, aligned parallel along the plume axis) were installed on two two translation stages mounted on the large CORONA vacuum chamber at ESA-ESTEC (2 m in diameter and 4 m in length). The first translation stage was mounted on the chamber rotating arm, allowing to scan angular position from $-20°$ to $+90°$ at distances between 550 to 750 mm from the thruster, while the second translation stage was placed further downstream, providing measurements along the plume axis 850 mm to 1550 mm from the thruster exit. The current-voltage characteristic (i.e. I-V curve) of the Langmuir probe was measured using a Keithley 2440 sourcemeter, sweeping the probe voltage from -15 V to $+35$ V. The plasma parameters, namely the electron density n_e, the electron temperature T_e and the plasma potential ϕ, were derived from the I-V curve both by fitting the appropriate expression of the current and by using the Druyvesteyn method [12]. Figure 1 shows an example of measured electron density and temperature in the plume region, for a discharge voltage of 300 V and a mass flow rate of 4 mg/s. With the exception of operating point B, which showed noisy measurements, the rest of cases have smooth axial profiles of electric potential ϕ and electron density n_e. The obtained values of electron temperature T_e also present smooth variations, except for cases B, E and F.

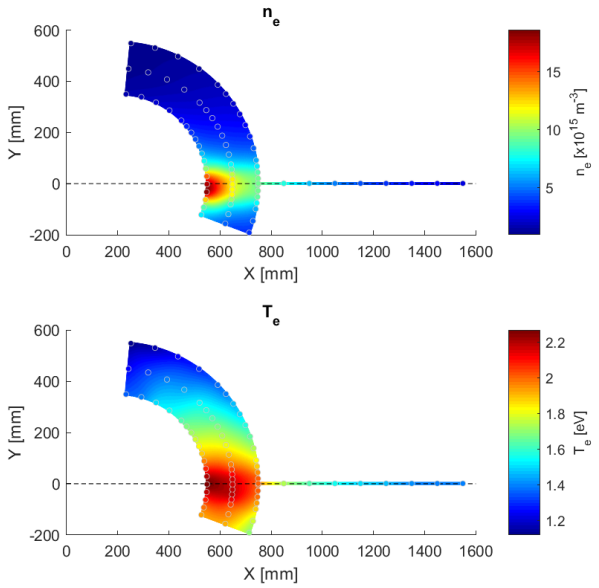

FIG. 1. Maps of the electron density n_e (top) and electron temperature T_e (bottom) for a discharge voltage of 300 V and a mass flow rate of 4 mg/s (case F). The SPT-100-ML thruster was position at the origin, with the plume direction along positive x. The dots show were measurements were performed and a 2D interpolation is displayed in-between.

Faraday cup (FC) measurements were used in the test campaign to obtain the angular distribution of the ion current density in the plasma plume. Details about FC design and operation can be found in [13]. The graphite probe collimator aperture is 10 mm in diameter; it defines the collection area. The cup is 16 mm in diameter and 20 mm in length. Electrical insulation between the cup and the collimator is achieved with PEEK spacers. The FC is mounted onto a floating aluminum holder fixed to the chamber rotating arm. The FC faces the center of

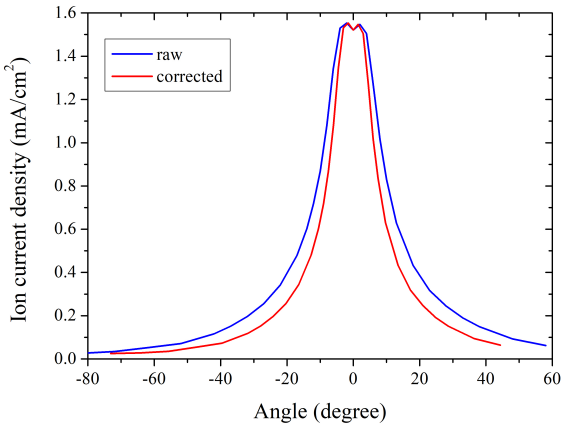

FIG. 2. Ion current density distribution measured for 300 V, 4 mg/s (case F). Raw and corrected profiles are shown.

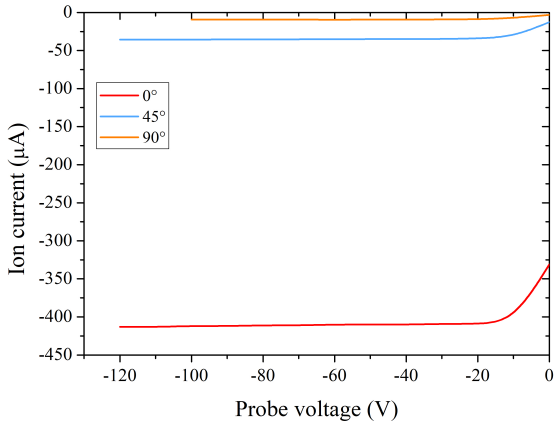

FIG. 3. Current to voltage curve for the Faraday probe measured at different angles from the centerline.

the thruster exit plane, i.e. it is parallel to ion current streamlines. The HT to probe distance is $x_F = 797$ mm. The current was recorded with a Keithley 2400 calibrated sourcemeter. The latter is also used to polarize the cup at -100 V for all measurements. The FC was positioned in the horizontal plane that contains the SPT-100-ML Hall thruster centerline. Ion current density measurements were performed over a hemisphere. In this work the Hall thruster was not aligned with the rotating arm pivot. As a consequence, the FC angle with respect to the thruster exit plane does not correspond to the arm angle, but at 0° when the arm is aligned with the thruster axis. Correction has been applied to all measured current angular distributions to retrieve the effective distributions. Figure 2 shows raw and corrected ion current density angular profiles for case F.

Figure 3 shows the current-voltage curve at various angles. The results show the great advantage of using Faraday Cups to measure the ion current density, since the saturation current does not depend on the voltage. This means the plasma sheath expansion effect is cancelled; thus current density measurements are more accurate with FCs compared to other probe types.

IV. COMPARISON RESULTS

The procedure used to compare the experimental results with the model can be summarized as follows. Firstly, the available experimental data for each operating point is prepared for the comparison. Since the spatial locations where the Faraday cup data and the Langmuir probe data were obtained are not identical, interpolation is carried out when needed to evaluate a plasma property. Also, the average of the plasma properties obtained from Langmuir probe measurements processed with the IV-curve method and the Druyvesteyn method is computed and used as the reference data for the model validation, after checking that the differences between the two are small.

Secondly, we determine the input parameters of the model for each case. The value of M_{i0} is obtained by using the ion current density from the Faraday probe at point F, $x_F = 797$ mm, i.e., $j_i(x_F)$. The value of $n_e(x_F)$ at that point is then interpolated from the Langmuir probe data, and ion velocity is determined as $u_i(x_F) = j_i(x_F)/n_e(x_F)$. Next, the ion velocity at the most upstream point L where measurements exist, $x_L = 550$ mm, is computed with the energy equation,

$$u_i(x,0) = \sqrt{u_i^2(x_F) - 2e\Delta\phi(x,0)/m_i} \qquad (7)$$

at $x = x_L$, where $\Delta\phi(x,0) = \phi(x,0) - \phi(x_F,0)$, with $\phi(x_F,0)$ interpolated from the Langmuir probe data at x_F. Finally, the ion Mach number for the kinetic model is computed as $M_{iL} = u_i(x_L)/\sqrt{T_e(x_L)/m_i}$, where $T_e(x_L)$ is obtained from Langmuir probe data. Under the assumption that the ions are hypersonic, so that Mach number variations along the plume axis are small, the initial Mach number is estimated as $M_{i0} = M_{iL}$. The values leading to this calculation and the resulting M_{i0} are shown in rows 3–8 and row 9 of table I for each experimental case. In the six test cases studied here, M_{i0} is in the range of 9–15. While the ion Mach number M_{i0} is one of the main input parameters of the kinetic model, analysis shows that the sensitivity to this parameter is large only for low values of M_{i0}, and that when the plume is hypersonic (say, $M_{i0} > 5$), the model results are only weakly dependent on the value of M_{i0}. Therefore, the dimensionless simulation results do not vary much among the different test cases. In the nomenclature used in reference [4], all cases have $\chi \simeq 0.02$.

As it can be observed, electron density n_e, ion velocity u_i, electric potential ϕ, and electron temperature T_e increase with the discharge voltage V_d, with the exception

of case B, which has the worst quality experimental results and is slightly off this trend. The increase of n_e can be attributed to a less divergent plume as V_d increases. The estimated ion velocity at x_F following the procedure above is seen to be consistent in all cases with the estimation based on the discharge voltage $u_i \approx \sqrt{2\beta e V_d/m_i}$, with $\beta \in$[0.4-1]. Lastly, it is seen that electron density n_e increases and u_i decreases with increasing $\dot{m}$, while there is no clear trend with $\dot{m}$ for ϕ and T_e. The behavior of the ion Mach number M_{i0}, which results from the combination of the behavior of u_i and T_e, is also non-trivial; however, overall it can be stated that it increases with the discharge voltage, V_d.

Thirdly, the beam width function, $h(x)/h(x^P)$, is computed from the experimental data using the paraxial continuity equation:

$$\frac{h^2(x)}{h^2(x^P)} = \frac{n_e(x^P)u_i(x^P)}{n_e(x,0)\sqrt{u_i^2(x^P) - 2e\Delta\phi(x,0)/m_i}} \tag{8}$$

where $\Delta\phi(x,0) = \phi(x,0) - \phi(x^P,0)$. The beam width function was inspected for all test cases and seen that it could be accurately approximated as a straight line in the measurement region with a relative RMS error of less than 0.1%. This is consistent with a nearly-conical expansion in the far plume region. Hence, a linear $h(x)$ fit with a constant slope $\mathrm{d}h/\mathrm{d}x$ (dependent on the operating case) is used in the comparison in the range where experimental data are available. The value of $\mathrm{d}h/\mathrm{d}x$, which represents the plume divergence rate, is seen to decrease with increasing discharge voltage V_d. This is consistent with a more collimated plasma beam as the discharge voltage increases.

Fourthly, the remaining parameters of the model, i.e., $h(x^P)$, ϕ_0, n_{e0}, and C, are determined for each test case by minimizing the mean square error in potential, density and temperature with the experimental data at the plume axis, for all points between 550 and 1550 mm from the thruster exit plane where Langmuir probe data are available. These parameters are shown in rows 10–14 of table I. With the exception of the previously mentioned noisy case B, the general trend of the upstream potential, ϕ_0, and electron density, n_{e0}, is to increase with the discharge voltage as could be expected.

It should be noted that the kinetic model returns the axial, radial, and azimuthal electron temperature T_{ex}, T_{er}, $T_{e\theta}$ as distinct values, showing the development of electron anisotropy in the expansion even if the distribution is initially Maxwellian. As separate temperature component data is not experimentally available, only the average temperature $T_e = (T_{ex}+T_{er}+T_{e\theta})/3$ can be used in this comparison study.

Once all the model parameters are fixed, simulations have been carried out for each experimental case. Below, the comparison and discussion of results is presented.

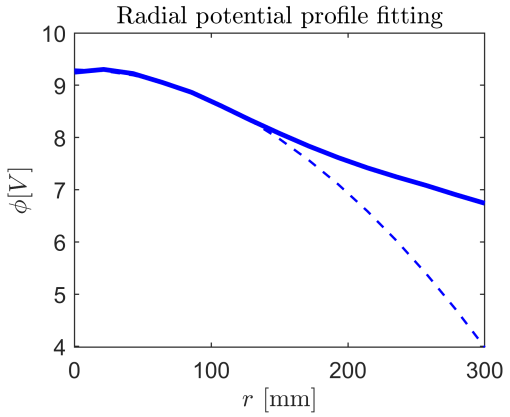

FIG. 4. Radial electric potential profile at $x = 550$ mm, the first plane of the plume where experimental data are available, for test case A. The thick line shows the interpolated experimental profile. The dashed line shows the approximated radially-parabolic electric potential profile used by the kinetic model.

A. Radial electric potential profile

One of the hypotheses of the kinetic model is that the electric potential profile ϕ has a parabolic shape in the radial direction. The radial electric potential profile at $x_1 = 550$ mm is shown in Figure 4 for test case A. This figure is representative of the rest of test cases, which are not shown in the sake of conciseness. As it can be observed, the experimental data are well approximated by the parabolic electric potential profile up to about $y = 150$ mm; from there outward, the measured potential decreases at a lower rate than the one considered in the model.

As the majority of the electron population has low energy E, most of the electrons cannot travel to large values of r, and hence they do not perceive the the difference between the radially-parabolic and the measured electric potential. The deviation from a radially-parabolic electric potential profile is expected to introduce an error in the model due to the change in the mathematical expression of the radial action integral, J_r, of the higher-energy electrons that can travel far in the radial direction before being radially reflected. In essence, the higher value of the potential at large r means that those electrons with high J_r will display a larger radial oscillation period than in the parabolic case. Future work must assess the importance of this assumption further by considering other radial profiles for the electric potential model.

B. Plasma properties along the plume axis

Figures 5, 6 and 7 compare the electric potential ϕ, the electron density n_e, and the electron temperature T_e between the fitted model and the experimental results in the region of measurement for all test cases A through

TABLE I. Operationg conditions (rows 1–2), experimental and intermediate data (3–8), fitted model parameters 9–14 and results (15–18) for cases A through F.

	A	B	C	D	E	F
V_d [V]	150	225	300	400	150	300
$\dot{m}$ [mg/s]	2	2	2	2	4	4
$n_e(x_F)$ [10^{15} m^{-3}]	1.29	2.59	2.77	3.30	4.78	7.29
$u_i(x_F)$ [m/s]	14484	15691	18000	24576	11759	12840
$\phi(x_F)$ [V]	7.22	7.68	9.58	10.21	7.73	10.31
$\phi(x_L)$ [V]	9.25	9.15	12.35	13.17	8.45	12.70
$u_i(x_L)$ [m/s]	14381	15622	17886	24488	11714	12702
$T_e(x_L)$ [eV]	2.86	1.96	3.57	3.66	1.44	2.60
M_{i0} [-]	9.92	13.02	11.04	14.94	11.40	9.19
$h(x_F)$ [mm]	301.5	155.6	123.3	76.7	254.3	82.23
$\mathrm{d}h/\mathrm{d}x$ [-]	0.301	0.144	0.135	0.088	0.22	0.09
ϕ_0 [V]	24.83	14.69	33.15	56.12	12.61	28.56
n_{e0} [10^{16} m^{-3}]	8.48	3.96	17.6	45.2	5.08	46.8
C [Vmm^2]	7385.4	4811.8	1688.9	551.45	14274	567.43
T_{e0} [eV]	4.81	2.77	6.55	12.04	2.20	4.98
ϕ_∞ [V]	1.28	1.95	1.79	2.43	2.17	3.73
$\bar{\gamma}$[−]	1.27	1.29	1.28	1.31	1.28	1.26

F. We can conclude that the potential, electron density, and electron temperature on the plume axis are well described by the model in all cases, which supports the validity of the model. The comparison error in electric potential is below 0.5 V everywhere, with the sole exception of a small region of case D. This error is below 10–20% of the local value of T_e in all cases, except in the noisy simulation B where it reaches 30%. The relative error of electron density n_e is less than 5–10% in all the experimental cases.

Regarding the electron temperature measurements, they are more noisy than the other variables. This is evident from the erratic experimental curves in these figures, especially in cases B, D, E. Notwithstanding this, the model clearly reproduces the average trend of the experimental data, which clearly proves that electron cooling is taking place in the near-collisionless expansion, which is one of the major predictions of the kinetic model. It is worth noticing that the experimental error in the electron temperature T_e affects the determination of constant C in the model, a fundamental sizing parameter for the radial electric potential profile, and thus an error in its determination affects the electric potential and electron density as well. Since the parameter fitting procedure followed here ensures that the error is as small as possible in ϕ, the electron density n_e, and the electron temperature T_e simultaneously, these three fits are not independent from each other.

The differences between model and experiment are in all cases comparable to the expected experimental error of a Langmuir probe in a plasma thruster plume, and indeed, most of the differences have a noisy oscillatory behavior, which can be attributed to the measurements themselves.

C. Model extrapolation to $x = 0$ and $x = \infty$

The model can be extrapolated in each test case to $x = 0$ and $x = \infty$ to investigate additional aspects of the plume expansion and further validate it. In the experiments, the thruster was electrically floated with respect to the vacuum chamber walls, to which the potential is referenced ($\phi = 0$). Two major difference between the free plasma expansion in space and in a vacuum chamber are the higher background pressure and the limited plume length in the latter case. These effects make it more difficult to validate the kinetic model with laboratory experiments. It is noted that the validity of the model relays on the expansion being non-magnetized and collisionless. Thus, as the model is extrapolated toward the exit plane of the thruster ($x = 0$), the error committed is expected to increase, as these assumptions are not longer satisfied there. In fact, it is not expected that $h(x)$ has the same slope $\mathrm{d}h/\mathrm{d}x$ in this near region as in the far region. Notwithstanding this, the model can be used to estimate ϕ_0, n_{e0}, and T_{e0}, the upstream values of the electric potential, electron density, and the electron temperature. Indeed, the former two were obtained as part of the parameter fitting process in Section IV and the three of them are shown in table I. These values roughly correspond to the potential, density and temperature close to the thruster, but they cannot be directly related to any specific location for the reasons above. As it can be observed, with the exception of test case B, ϕ_0, n_{e0} and T_{e0} increase with increasing discharge voltage V_d. Increasing the Xenon mass flow rate increases the electron density n_{e1}. However, it also increases the background pressure in the vacuum chamber, which translate into a larger plasma collisionsionality. This goes against the collisionless assumption in the kinetic model, so it can be expected that cases E and F will be worse represented

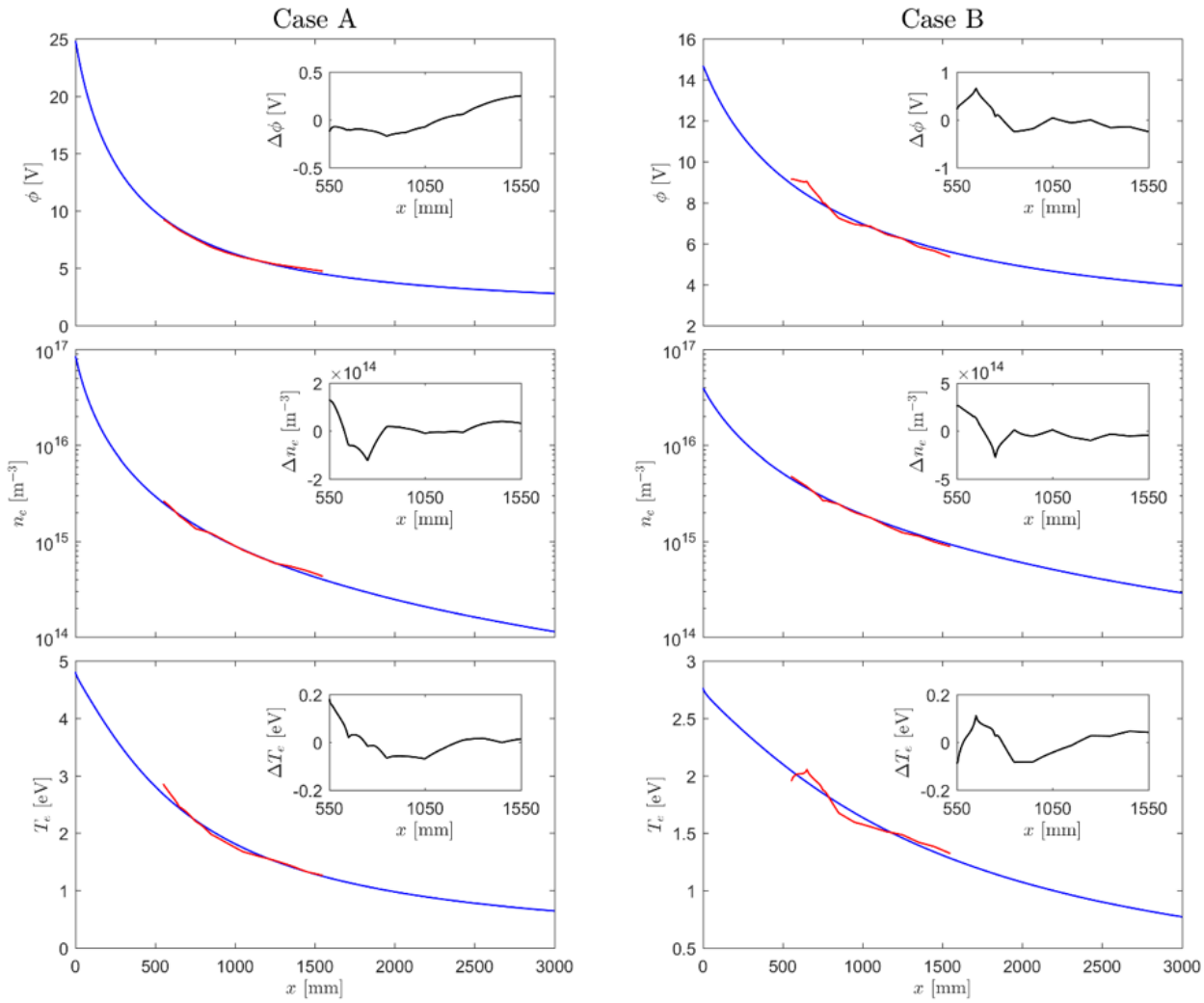

FIG. 5. Experimental (red segment lines) and fitted model (blue lines) curves for the plasma potential, ϕ, electron density n_e, and electron temperature T_e, along the plume axis (y=0), for test cases A and B. The difference between the two lines in the region of measurement is displayed in the inset plots.

by the model.

While in the laboratory the presence of the chamber wall interrupts the plasma expansion to infinity, the plasma forms a sheath at the chamber wall downstream to ensure a net current-free plume, such that the total potential fall from the thruster to the chamber wall, i.e., including the sheath, is essentially the same as the total potential fall in space from the thruster to infinity. In other words, ϕ_∞ should roughly correspond to the potential of the vacuum chamber, $\phi = 0$. As it can be observed in table I, ϕ_∞ is slightly greater than 0 in all test cases, but within one electron temperature T_{e0} from it, i.e., $e\phi_\infty/T_{e0} < 1$. This consistency further supports the validation of the model.

V. APPROXIMATE FLUID CLOSURE LAW

As previously mentioned, most of the existing plasma plume simulation codes follow a fluid description for the electrons and many of them use as closure relation a simple law relating the electron density and temperature by means of a simple polytropic exponent, γ, i.e., $T_e = T_{e0}(n_e/n_{e0})^{\gamma-1}$. The kinetic results of the model of reference [4] can be used to compute an approximated, *effective* electron polytropic cooling exponent $\bar{\gamma}$ for each experimental case. The value of $\bar{\gamma}$ can be chosen to give the same potential fall $\phi_\infty - \phi_0$ along the plume as in the kinetic model. Integrating the collisionless electron momentum equation $0 = -\partial(n_e T_e)/\partial x + e n_e \partial\phi/\partial x$ between

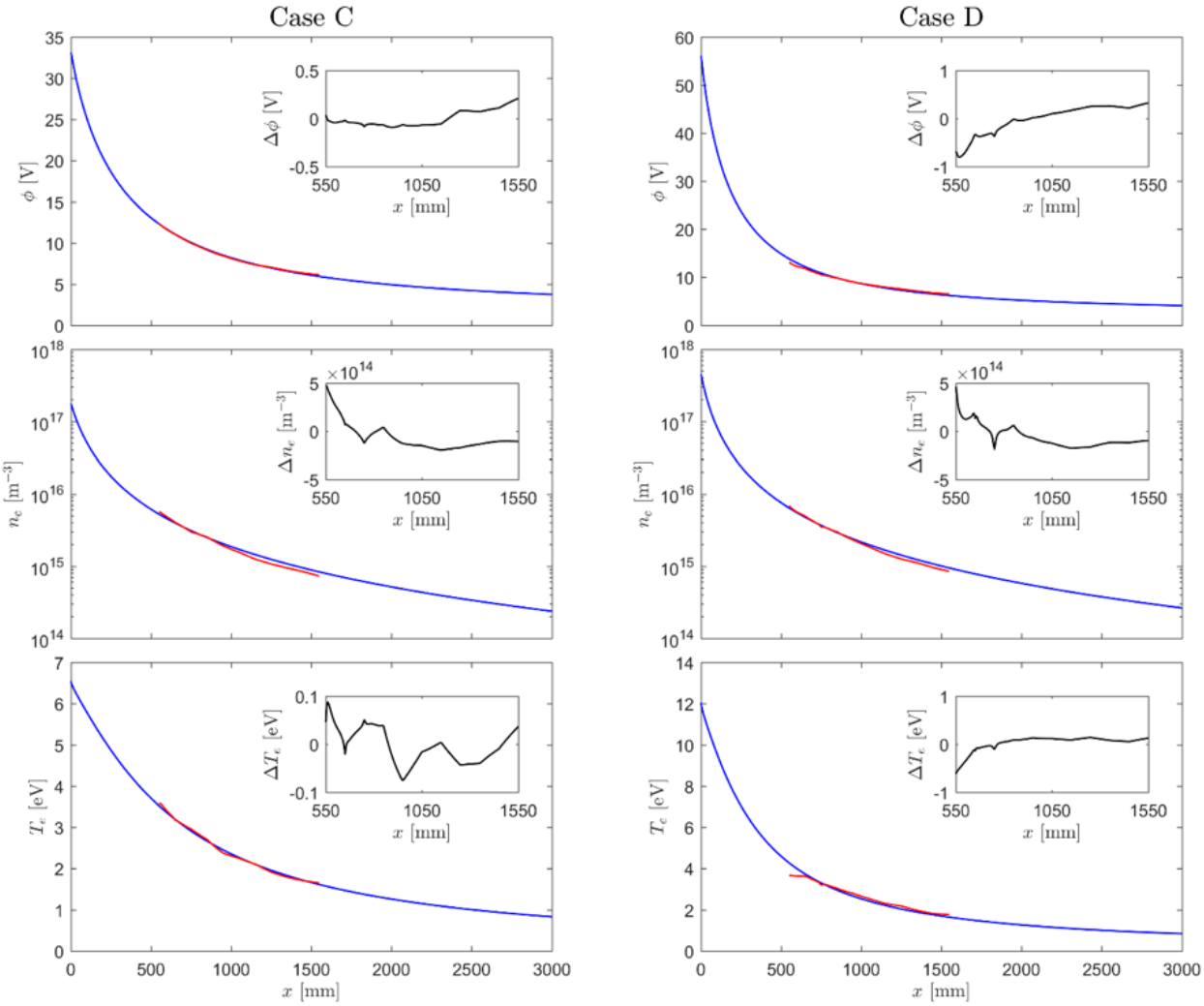

FIG. 6. Experimental (red segment lines) and fitted model (blue lines) curves for the plasma potential, ϕ, electron density n_e, and electron temperature T_e, along the plume axis (y=0), for test cases C and D. The difference between the two lines in the region of measurement is displayed in the inset plots.

$x = 0$ and $x = \infty$,

$$\bar{\gamma} = \frac{\mid \phi_\infty - \phi_0 \mid}{\mid \phi_\infty - \phi_0 \mid - T_{e0}/e}. \tag{9}$$

The last row of table I presents the values of effective $\bar{\gamma}$ for the considered conditions. The value of this effective, lumped-model polytropic cooling exponent $\bar{\gamma}$ is in the range [1.26-1.31] for all cases. There is no clear trend to the behavior of this parameter with the discharge voltage or the propellant mass flow rate. These values are in line to those reported experimentally by [9] for the same experiments. They are also in agreement with the measured values in a PPS-1350-ML and a PPS-100-ML [14], as well as a BHT-200 [15] in the far plume region.

Finally, while it might provide a first approximation to the plasma expansion, it should be noted that a lumped model like this one conceals the local variation of the cooling rate in the collisionless expansion, which does not fit well with a single polytropic exponent. And although the value of ϕ_∞ is correctly captured by a polytropic approximation (indeed, $\bar{\gamma}$ has been defined to match ϕ_∞, the local electric potential map in the plume differs substantially from that of the kinetic model [16]. Moreover, a simple polytropic model neglects the anisotropy in electron temperature that develops as the collisionless electrons expand [4].

VI. CONCLUSIONS

The kinetic electron model of a paraxial, unmagnetized, collisionless plasma plume expanding into vacuum of [4] has been compared against the six experimental test cases of a SPT-100-ML Hall Effect Thruster from

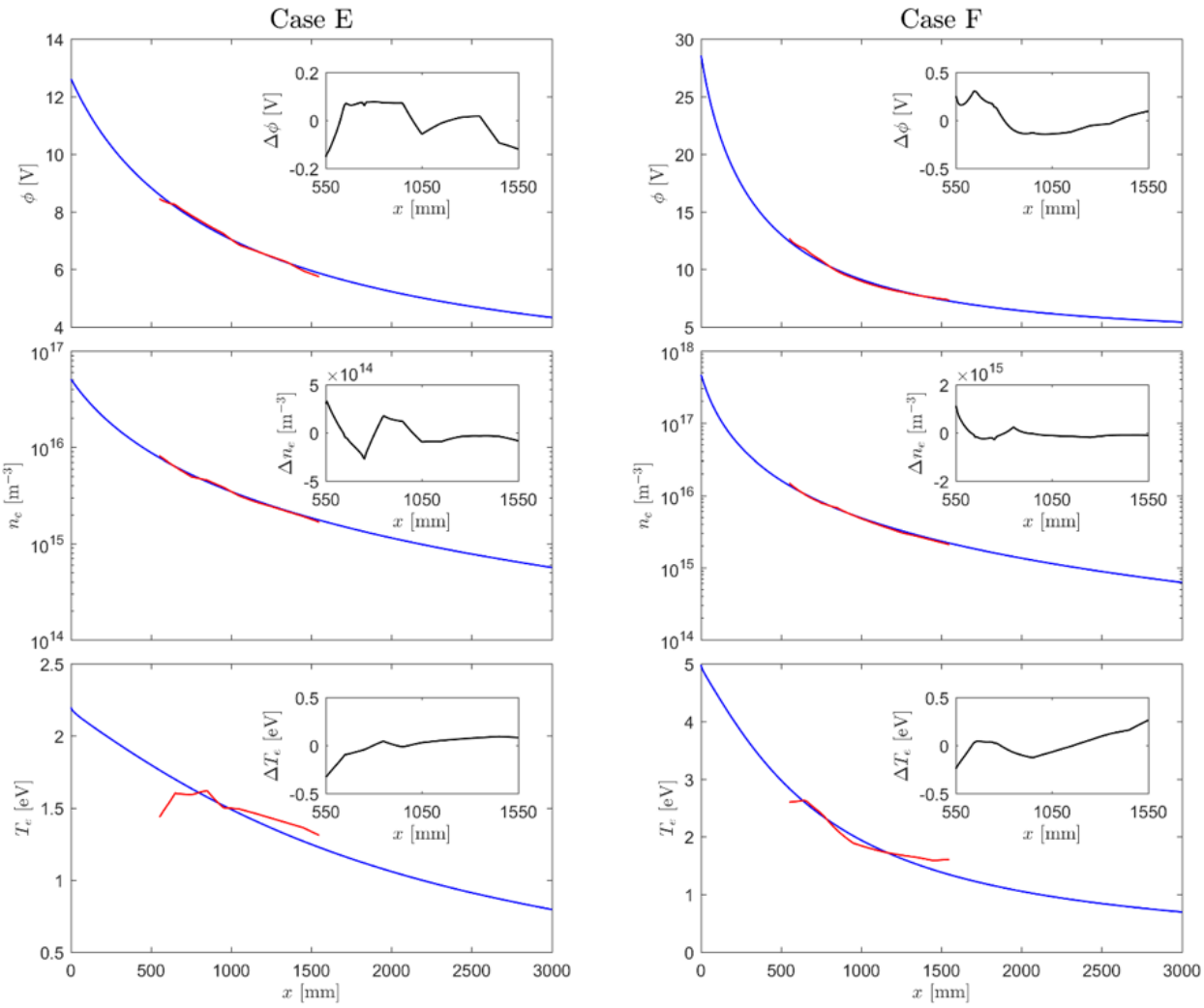

FIG. 7. Experimental (red segment lines) and fitted model (blue lines) curves for the plasma potential, ϕ, electron density n_e, and electron temperature T_e, along the plume axis (y=0), for test cases E and F. The difference between the two lines in the region of measurement is displayed in the inset plots.

[9]. A comparison procedure has been established that first computes the input parameters of the model M_{i0}, $\mathrm{d}h/\mathrm{d}x$ for each test case and then fits the normalization constants (ϕ_0, n_{e0} and C) to minimize the difference error. The kinetic model, which follows exploits the conservation of mechanical energy, angular momentum about the plume axis and the adiabatic radial action integral to solve the electron Vlasov's equation is seen to match well the laboratory measurements. This is a first step toward the validation of the model; additional and more detailed measurements, such as of the electron temperature anisotropy in the plume, are necessary to assess the accuracy of all the predictions of the model and fully validate it.

The accuracy of the radial parabolic potential profile used by the model has been confronted against real data, showing good agreement in the central part of the plume, and increasing differences in the plume radial periphery. The deviation from the assumed profile introduces a computation error in the the radial action integral of electrons, J_r, which is expected to affect only high energy electrons, i.e., only a minority of the population. Kinetic models with other radial potential profiles, closer to the measured ones, can be developed to better approximate this aspect of the problem.

The agreement on the fundamental plasma parameters along the plume axis (potential ϕ, electron density n_e, and electron temperature T_e) has been evaluated and discussed using the available measurements, in the range $x = 550$–1550 mm. The error in potential and electron density is small in all six test cases and within experimental uncertainty. The evolution of T_e clearly follows the trend recovered experimentally, but the measurements are noisier.

The departure of the laboratory test conditions from in-space conditions presents a surmontable hurdle toward the validation of the model. In particular, the higher background pressure and presence of the vacuum chamber wall that interrupts the plume expansion to infinity can affect the results of the comparison. It is noted that the electron response in the collisionless plume is global, meaning that an effect downstream can alter the expansion upstream, and vice-versa. However the model shows a fitted $\phi_i nfty$ value that is only slightly higher than 0, consistent with the potential of the vacuum chamber wall.

Finally, an approximated, effective electron polytropic coefficient was computed that gives the same total potential fall than the model. The values computed for the different operating conditions tested are in the range $\bar{\gamma}_e = 1.26$–1.31, in agreement with other values reported in the literature.

ACKNOWLEDGMENTS

The authors would like to thank the support and use of the facilities at the Electric Propulsion Laboratory at ESTEC. This work was performed in the framework of the 'Model and Experimental validation of spacecraft-thruster Interactions (erosion) for electric propulsion thrusters plumes' (MODEX) project (ESA contract number 4000116180/15/NL/PS). MODEX is a collaboration between Airbus-DS, UC3M, ONERA, CNRS-ICARE and KTH aiming to provide a better understanding of the plasma properties in the farplume of a Hall thruster. Additional funding for M. Merino and P. Fajardo came from Project ESP2016-75887 (Spain's National Research and Development Plan - MINECO/FEDER).

[1] E Tverdokhlebova and AG Korsun. Plasma plume/spacecraft interaction. state of the art in investigation methodology. In *Spacecraft Propulsion*, volume 465, page 675, 2000.

[2] ID Boyd and A. Ketsdever. Interactions between spacecraft and thruster plumes. *Journal of Spacecraft and Rockets*, 38(3):380, 2001.

[3] D.M. Goebel and I. Katz. *Fundamentals of Electric Propulsion: Ion and Hall Thrusters*. Jet Propulsion Laboratory, Pasadena, CA, 2008.

[4] Mario Merino, Javier Mauriño, and Eduardo Ahedo. Kinetic electron model for plasma thruster plumes. *Plasma Sources Science and Technology*, 27(3):035013, 2018. doi:10.1088/1361-6595/aab3a1.

[5] Mario Merino and Javier Mauriño. AKILES code: Advanced Kinetic Iterative pLasma Expansion Solver 2D, DOI: 10.5281/zenodo.1098432, 2017. doi:10.5281/zenodo.1098432.

[6] Filippo Cichocki, Adrián Domínguez-Vázquez, Mario Merino, and Eduardo Ahedo. Hybrid 3D model for the interaction of plasma thruster plumes with nearby objects. *Plasma Sources Science and Technology*, 26(12):125008, 2017.

[7] Jean-FranÇois Roussel, FranÇois Rogier, Guillaume Dufour, Jean-Charles Mateo-Velez, Julien Forest, Alain Hilgers, David Rodgers, Laurence Girard, and Denis Payan. SPIS open-source code: Methods, capabilities, achievements, and prospects. *IEEE Transactions on Plasma Science*, 36(5):2360–2368, 2008.

[8] Gabriel Giono, Stéphane Mazouffre, Dimitry Loubere, Lara Popelier, Christophe Théroude, Käthe Dannenmayer, Fabien Marguet, Jón Gudmundsson, Nickolay Ivchenko, Georgi Olentsenko, and Mario Merino. Experimental determination of the plasma properties in the far-plume of an SPT-100 hall thruster. In 35^{th} *International Electric Propulsion Conference*, number IEPC-2017-385 in IEPC-2017-385, Atlanta, GA, 2017. Electric Rocket Propulsion Society.

[9] Gabriel Giono, Jón Gudmundsson, Nickolay Ivchenko, Stephane Mazouffre, Käthe Dannenmayer, Lara Popelier, Dimitry Loubere, Mario Merino, and Georgi Olentsenko. Non-maxwellian electron energy probability functions in the plume of a SPT-100 hall thruster. *Plasma Sources Science and Technology*, 27(1):015006, 2018. doi:10.1088/1361-6595/aaa06b.

[10] Herbert Goldstein, Charles P Poole, and John L Safko. *Classical mechanics*. Pearson, 2001.

[11] Gonzalo Sánchez-Arriaga, Jiewei Zhou, E Ahedo, Manuel Martínez-Sánchez, and Jesús José Ramos. Kinetic features and non-stationary electron trapping in paraxial magnetic nozzles. *Plasma Sources Science and Technology*, 27(3):035002, 2018.

[12] M.A. Lieberman and A.J. Lichtenberg. *Principles of plasma discharges and materials processing*. John Wiley and Sons, Hoboken, NJ, 2005.

[13] S Mazouffre, G Largeau, L Garrigues, C Boniface, and K Dannenmayer. Evaluation of various probe designs for measuring the ion current density in a hall thruster plume. In *35th International Electric Propulsion Conference*, pages 1–17, 2013.

[14] K Dannenmayer and Stéphane Mazouffre. Electron flow properties in the far-field plume of a hall thruster. *Plasma Sources Science and Technology*, 22(3):035004, 2013.

[15] M. Nakles, L. Brieda, G. Reed, W. Hargus, and R. Spicer. Experimental and numerical examination of the BHT-200 Hall thruster plume. In *43rd AIAA/ASME/SAE/ASEE Joint Propulsion Conference & Exhibit*, page 5305, Washington DC, 2007. American Institute of Aeronautics and Astronautics, Reston, VA.

[16] Judit Nuez, Mario Merino, and Eduardo Ahedo. Fluid-kinetic propulsive magnetic nozzle model in the fully magnetized limit. In 36^{th} *International Electric Propulsion Conference*, number IEPC-2019-254, Vienna, Austria, 2019. Electric Rocket Propulsion Society.